HHS Public Access

Author manuscript

Mater Sci Eng C Mater Biol Appl. Author manuscript; available in PMC 2020 September 01.

Published in final edited form as:

Mater Sci Eng C Mater Biol Appl. 2019 September ; 102: 1–11. doi:10.1016/j.msec.2019.04.026.

Enhanced cell functions on graphene oxide incorporated 3D printed polycaprolactone scaffolds

Janitha M. Unagolla[a] and **Ambalangodage C. Jayasuriya**[a,b,*]

[a]Biomedical Engineering Program, Department of Bioengineering, College of Engineering, University of Toledo, Toledo, OH 43607, USA

[b]Department of Orthopedic Surgery, College of Medicine and Life Sciences, University of Toledo, Toledo, OH 43614, USA

Abstract

For tissue engineering applications, a porous scaffold with an interconnected network is essential to facilitate the cell attachment and proliferation in a three dimensional (3D) structure. This study aimed to fabricate the scaffolds by an extrusion-based 3D printer using a blend of polycaprolactone (PCL), and graphene oxide (GO) as a favorable platform for bone tissue engineering. The mechanical properties, morphology, biocompatibility, and biological activities such as cell proliferation and differentiation were studied concerning the two different pore sizes; 400 μm, and 800 μm, and also with two different GO content; 0.1% (w/w) and 0.5% (w/w). The compressive strength of the scaffolds was not significantly changed due to the small amount of GO, but, as expected scaffolds with 400 μm pores showed a higher compressive modulus in comparison to the scaffolds with 800 μm pores. The data indicated that the cell attachment and proliferation were increased by adding a small amount of GO. According to the results, pore size did not play a significant role in cell proliferation and differentiation. Alkaline Phosphate (ALP) activity assay further confirmed that the GO increase the ALP activity and further Elemental analysis of Calcium and Phosphorous showed that the GO increased the mineralization compared to PCL only scaffolds. Western blot analysis showed the porous structure facilitate the secretion of bone morphogenic protein-2 (BMP-2) and osteopontin at both day 7 and 14 which galvanizes the osteogenic capability of PCL and PCL + GO scaffolds.

Graphical abstract

[*]Author of Correspondence: Ambalangodage C. Jayasuriya, Ph.D., University of Toledo, Department of Orthopaedic Surgery, 3065 Arlington Avenue, Dowling Hall # 2447, Toledo, OH 43614-5807, USA, Tel: 419-383-6557, Fax: 419-383-3526, a.jayasuriya@utoledo.edu.

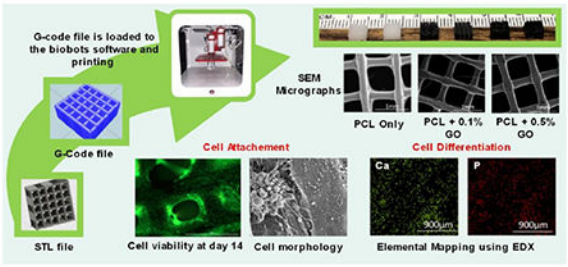

Keywords

Polycaprolactone; graphene oxide; biocompatibility; cell proliferation; differentiation

1. Introduction

The ideal scaffold for bone tissue engineering has to fulfill the number of requirements, such as (i) a three dimensional, porous structure with suitable surface chemistry to support cell attachment and proliferation, (ii) an interconnected pore structure for mass transport (nutrient and waste), (iii) a biocompatible, bioresorable substrate with balanced degradation rate with tissue ingrowth, and maintained integrity during degradation, and (iv) have mechanical properties similar to the tissue at the site of implantation [1–4]. Further, the appropriate pore size is important for the vascularization [5] and extracellular matrix production [6]. Various techniques, including gas forming, solvent casting, salt leaching, membrane lamination, and fiber binding have been used for the fabrication of 3D scaffolds [1,7,8]. However, the inability to make uniform interconnected porous structure and difficulty in controlling the shape of the scaffold and pore size limits the usage of the above methods in 3D scaffolding. 3D printing can be utilized for its versatility and its ability to make precise scaffolds with interconnected pore structure. The size and shape of the pores can be easily changed with high repeatability.

Many synthetic polymers such as poly (L-lactic acid) (PLA) [9], poly(L-lactic-co-glycolic acid) (PLGA) [10], polycarbonate (PC) [11], acrylonitrile butadiene styrene (ABS), poly (ε-caprolactone) [12], and poly (ethylene glycol) (PEG) [8,13] have been used for 3D printing. Polycaprolactone (PCL), an aliphatic polyester, has been extensively studied for tissue engineering applications due to its good biocompatibility, and low immunogenity. Also, the 6-hydroxyhexanoic acid, the degradation product of PCL is a naturally occurring metabolite in the human body [14]. Further, the degradation product is less acidic as compared to other types of aliphatic polyester, such as polyglycolide (PGA) and PLA [15]. Due to the extensive *in vitro* and *in vivo* biocompatibility and efficacy studies, PCL was approved by the US food and drug administration (FDA) to use in a number of medical and drug delivery devices [2,16]. PCL is a promising material in bone tissue engineering field due to its high mechanical strength and the low melting point [12]. However, pure PCL is hydrophobic solid, lacking functional groups which result in lower cellular response [14]. Most commonly used the method to increase the hydrophilicity is the incorporating inorganic substances such as nano-hydroxyapatite (nHA) [3], β-tricalcium phosphate [17], and graphene oxide (GO) [18].

Graphene, a single layer of aromatic carbon atoms in a two-dimensional honeycomb lattice, and its derivatives have attracted significant attention because of their unique physicochemical properties as a potential biomaterial [18–21]. The hydrophobic nature of the graphene results in the formation of agglomerations due to the strong $\pi - \pi$ stacking interaction [22,23], but the GO; one of the most important derivatives of graphene has high Young's modulus, excellent flexibility, and also hydrophilic oxygen-containing groups such as epoxy, carboxyl, and hydroxyl on its surface; plays an important role. GO is an excellent biomaterial for regulating cell function [24], and loading and releasing therapeutic drugs [25]. GO has attracted high interest in the field of bone tissue engineering in the last few years. The hydrophobic and electrostatic interaction [26,27] with proteins could potentially increase the osteogenic differentiation of progenitor cells and therefore promotes the osteogenesis [28].

GO incorporated PCL scaffolds have been previously studied by several researchers. The most widely used method of scaffold preparation was the electrospinning [18,29,30], and different solvent had been used to incorporate GO into PCL such as dichloromethane (DCM) [30], dimethylformamide (DMF) [31,32], chloroform [33], and a combination of both DCM and DMF [18,29]. GO was dissolved in DMF to obtain homogeneous suspension [30] and it was also reported that the surface tension of the mixed solution of GO was reduced by the DMF [18].

Apart from the electrospinning technique, covalently linked graphene PCL composites were prepared using the precipitation and washing up steps. GO chemically converted to an anhydrous dispersion of graphene to prevent aggregation and mixture (with PCL+DMF) was precipitated in cold methanol followed by filtration and drying in vacuum oven [31]. In addition to PCL, GO can be successfully incorporated to the number of natural and synthetic polymers such as chitosan [28], collagen [34], poly (lactic acid) (PLA) [29], poly (L4actic-co-glycolic acid) (PLGA) [21], and poly-L-lysine (PLL) [35].

The main objective of this research work was to incorporate GO into the PCL and make scaffolds using a 3D printing technique. Also, this type of GO incorporated 3D printed scaffolds was not studied well according to the past literature. In this study, both the effect of pore size and the effect of the amount of GO on the cell functions were studied using murine pre-osteoblasts. The cytotoxicity of the GO incorporated scaffolds were first studied to check the suitability of the process conditions. Further, the mechanical stability of the scaffolds with the two different pore sizes and two different GO amounts were tested. The morphology of the attached cells and the effect of GO on cell differentiation were also studied using western blot analysis for bone morphogenic protein-2 (BMP-2) and osteopontin markers at day 7 and 14.

2. Materials and Methods

2.1 Materials

Polycaprolactone (PCL) (MW: 50000kDa) was purchased from Allevi (Philadelphia, PA, USA). Graphene Oxide (GO) powder (15-20 sheets), chloroform (99.8% ACS reagent), hexamethyldisilazane (HMDS), β- glycerol phosphate disodium salt pentahydrate, L-

ascorbic acid, and cell proliferation reagent WST-1 (Roche diagnostic) were all purchased from Sigma Aldrich Chemicals (St. Louis, MO, USA). Alpha minimum essential media (α-MEM), Fetal Bovine serum (FBS), phosphate buffered saline (PBS), Dulbecco's phosphate buffered saline (DPBS), and penicillin/streptomycin were purchased from Gibco, life technologies (Thermo Fisher Scientific, USA). Live/Dead cell viability/cytotoxicity kit was purchased from the Invitrogen (USA). 2.5% glutaraldehyde in 0.1M sodium cacodylate buffer solution was purchased from electron microscopy sciences (Hatfield, PA, USA). Alkaline phosphate (ALP) assay kit was purchased from Biovision Incorporated (Milpitas, CA, USA).

2.2 PCL-GO Preparation

lg of PCL was added to the 5 ml of chloroform solution under continuous stirring at 600 rpm to obtain a fully dissolved PCL solution. 0.1% (w/w) and 0.5% (w/w) GO concentrations were achieved by adding 1 mg and 5 mg of GO, respectively, into the PCL solution. The system was stirred for 30 min to get a homogeneous suspension of GO powder and system was sonicated for 5 min. Then the mixture was heated up to 100°C to remove the solvent and remaining solid component was used to print the scaffolds.

2.3 Printing of the scaffolds

Scaffolds were printed by using extrusion-based Allevi2 3D bioprinter. A square shape (5×5 mm) mesh structures with two different pore sizes, 400 μm, and 800 μm, were developed using Autodesk Fusion 360 3D modeling software. For all the studies, cuboidal scaffolds with 2.2 mm thickness (22 layers) were generated as CAD models, exported as stereolithography (STL) files, and imported into Slic3r; an open source software used to generate machine-readable G-code files. The solid materials were filled to the stainless steel syringe with 30 gauge nozzle (inner diameter 0.159mm) and heated up to 100°C before printing. Printer was run at a linear speed of 1mm/s and printing pressure was kept at a range of 80-100 PSI. Scaffolds were printed using three material combinations such as PCL only, PCL with 0.1 % (w/w) GO, indicated as 0.1% GO, and PCL with 0.5 % (w/w) GO, indicated as 0.5% GO.

2.4 Testing of the compressive modulus of scaffolds

The scaffolds were subjected to a compression test using the ADMET expert 2600 series universal testing machine at a constant rate of 0.01 mm/s. Stress vs. strain graphs were obtained for each sample by using the force vs. displacement curve generated from the software. The compressive modulus was calculated by using the linear region (elastic region) of the stress vs. strain graphs. Seven samples were used for each sample type.

2.5 Morphological Analysis

The surface morphology of the scaffolds was examined using the scanning electron microscope (SEM) (FEI Quanta 3D FEG dual bean ESEM, USA) followed by gold-palladium supper coating at an accelerating voltage of 5 kV.

2.6 *In Vitro* cell culture

2.6.1 Scaffolds preparation and cell seeding—All the scaffolds were sterilized in 70% ethanol solution for 1 h and followed by thorough washing in 1× PBS solution three times. Finally, dried scaffolds were further sterilized under ultraviolet (UV) light for 30 min. Before cell seeding, scaffolds were incubated for 3 h in α-MEM growth medium at 37°C.

Murine preosteoblast cell line (OB6) was cultured in α-MEM medium containing 15% FBS, and 1% penicillin-streptomycin. The culture was maintained in a humidified incubator at 37°C with 5% CO_2 and the culture medium was replaced every 3 days. After 80% of confluency, the cells were digested and sub cultured using 0.25% trypsin EDTA. In this study, 40,000 cell density was used for each scaffold. To achieve proper cell adhesion to the scaffold, 300 μl of cell suspension was added to the each scaffold to barely cover the whole scaffold and incubated for 3 h. After 3 h, the emaining amount of α-MEM growth medium (700 μl) was added to the scaffolds. This procedure was carried out for all cell culture studies. For osteogenic differentiation studies, in addition to the α-MEM growth medium, 10 mM β-glycerol phosphate and 50 μg/ml L-ascorbic acid were added.

2.6.2 Live and dead cell viability assay—Live/dead (L/D) cytotoxicity assay was performed for cell seeded scaffolds at days 3, 7, and 14; according to the manufacturer protocol. Briefly, 5 μl of 4 mM calcine and 20 μl of 2 mM ethidium homodimer-1 were added to 10 ml of the 1× DPBS solution to make the L/D assay solution. After removing the α-MEM growth medium from each well, scaffolds were washed with 1× PBS twice and moved to a new 24 well plate. Then, 600 μl of prepared L/D assay solution and 600 μl of 1× DPBD were added to each scaffold and incubated at room temperature for 30min. Before imaging, 800 μl of the solution was removed from each well to eliminate the floating of the scaffolds. The top surface of the scaffolds was observed using cell imaging fluorescence microscopy (Cytation5, BioTek Inc, USA). Both live and dead cell images were processed and combined using Gen 3.03 software.

2.6.3 Cell proliferation—Water-soluble tetrazolium salts (WST-1) assay was used to quantify the cell proliferation by considering the fact that the cell enzyme activity is directly proportional to the number of metabolically active cells and it leads to the formation of formazan dye. All six types of scaffolds were seeded with 40,000 cells per well as described previously. The WST-1 assay was performed at days 3, 7, and 14. After each predetermined time points, the α-MEM medium was removed, and scaffolds were washed with PBS. Then the scaffolds were moved into the new 24-well plate, and the new α-MEM medium was added to each scaffold with 10% (v/v) WST-1 reagent. Blank samples that only contained scaffolds without cells with medium and WST-1 were also prepared. The well plates were shaken for 2 min at 300 rpm to make homogeneous mixing of WST-1 with the α-MEM medium. Then the scaffolds and blank samples were incubated for 6 h at 37°C and 5% CO_2. After 6 h, 100 μl from each well was transferred to 96-well plate and the level of dye formed was measured using spectrophotometer (SpectraMax190, Molecular Devices) at a wavelength of 440 nm. The optical density values from the scaffolds without cells were subtracted from each experimental values as a background.

2.6.4 Cell morphology and attachment—For morphological analysis of the cell attached scaffolds, the samples were washed with PBS after removing the medium and fixed with 0.6 ml of 2.5% glutaraldehyde in 0.1 M sodium cacodylate buffer solution for 30 min at 4 °C. After thorough washing twice with PBS, scaffolds were dehydrated through a series of graded ethanol concentrations (30%, 50%, 70%, 90% and 100%) and finally dried in HMDS. After proper drying, scaffolds were coated with gold and palladium using a sputter coater (Cressington 108 Auto) and were then observed using an SEM (FEI Quanta 3D FEG dual beam ESEM, USA) operated at an accelerating voltage of 5 kV.

2.7 Cell Differentiation

2.7.1 ALP Quantification—The amount of p-nitrophenol (pNP), dephosphorylated from p-nitrophenyl phosphate (pNPP) in the presence of ALP, was quantified using the ALP assay kit, in order to determine the cellular ALP activity. The cells were seeded to the scaffolds at 40000 cells/well as described previously and the assay was performed at days 3, 7, and 14. For the assay, the cell attached scaffolds were washed thoroughly with 1× PBS and transferred to microcentrifuge tubes. 300 μl of lysis buffer was added to the scaffolds and vortexed for 1 min to lyse the cells attached to scaffolds. Then, it was centrifuged at 13,000 g for 3 min, and the supernatant was collected and transferred to the new microcentrifuge tubes followed by a second centrifugation. The supernatant was collected and mixed with the pNPP substrate, and the kit procedure was followed. The color change was quantified using SpectraMax 190 microplate reader (Molecular Devices, USA) and the ALP activity was estimated according to the standard curve obtained from ALP enzyme supplied with the kit. The amount of ALP activity was normalized with the total protein content in each sample. Coomassie plus protein assay kit (Thermo Scientific, USA) was used to quantify the total protein as given in the kit protocol.

2.7.2 Energy dispersive X-ray (EDX) analysis- quantification of calcium and phosphorous—EDX analysis was done for elemental mapping of scaffolds using backscattered electron detector of SEM followed by gold-palladium sputter-coating at an accelerating voltage of 20 kV. The cells were fixed to the scaffolds using the same method as described in section 2.6.4. The percentage of calcium (Ca) and phosphorous (P) was determined according to the major four elements in the scaffolds namely carbon, oxygen, calcium, and phosphorus.

2.7.3 Western blot analysis—After 7 and 14 days of cell culture, attached cells were lysed with cell lysis buffer (Abeam, abl52163) containing 1mM phenylmethylsulfonyl fluoride (PMSF) as a protease inhibitor and protein amounts were quantified by the bicinchoninic acid (BCA) protein assay kit (Pierce, Thermo Scientific). Protein (10 μg) was then separated by sodium dodecyl sulfate (SDS) polyacrylamide gel electrophoresis and transferred to polyvinylidene fluoride (PVDF) membrane, and then membranes were blocked for 1 h in 5% (w/v) skim milk in tris-buffered saline (TBS) containing 0.1% Tween-20. Then the membranes were incubated against the primary antibodies: anti-bone morphogenic protein 2 (BMP-2, ab 14933, Abeam), anti-osteopontin (ab8448, Abeam) and anti-β actin as a housekeeping gene (#4970, Cell Signaling Technology) overnight at 4°C and a dilution of 1:1000. The membranes were further incubated with horseradish

peroxidase conjugated secondary antibody (#7074, Cell Signaling Technology) for 1 h at room temperature and a dilution of 1:2000 after rinsing three times in TBS-Tween 20, membranes were immersed in ECL substrate for 5min and then bands were visualized using G-box (Syngene, Frederick, MD, USA) with a exposure time of 2 min. The intensity of the protein bands was quantified using Image Studio Lite software.

2.8 Statistical Analysis

All data values in the graphs are presented as a mean ± standard error of the mean for each group of samples. For mechanical properties, seven samples were tested per group, and for swelling and cell culture studies, three samples were tested per group. One-way Analysis of Variance (ANOVA) was performed using IBM SPSS statistical software (version 21, IBM Company, Armonk, NY, USA) to determine the statistical difference. Post hoc Tukey's test was performed to determine the statistical difference between the groups. All tests were conducted with 95% confidence intervals ($p < 0.05$).

3. Results and Discussion

3.1 Mechanical properties

The compressive modulus of the scaffolds was tested using uniaxial compression test. As shown in Figure 2, the compressive modulus of 800 μm pore scaffolds was lower than the 400 μm pore scaffolds. The pore size of the scaffold dramatically effects to the compressive modulus. The lowest compressive modulus of 41.38 ± 4.69 MPa was obtained for PCL with 0.1% GO scaffold having 800 μm pores. However, the differences in compressive modulus between the three different scaffold groups with 800 μm pores were not statistically significant. The highest compressive modulus of 75.36 ± 4.07 MPa was reported on PCL only scaffolds with 400 μm pores, and the compressive modulus was decreasing with the increasing amount of GO without any statistical significance. The addition of GO neither improve nor reduce the compressive modulus of PCL scaffolds significantly. Since PCL itself shows a better compressive modulus, the addition of a tiny amount of GO, such as 0.1% (w/w), and 0.5% (w/w) does not give significant variation to the compressive modulus. The main controlling factors of compressive and tensile properties of this type of PCL scaffolds are the porosity and the molecular weight of the PCL [36].

3.2 Morphological analysis

Figure 3 represents the SEM micrographs of PCL only and PCL + GO scaffolds. The surface texture of the three scaffolds was slightly varied according to the composition. The PCL only scaffolds showed a comparatively rough surface with some irregularities, but Go contained scaffolds showed a smooth surface with GO particles on the surface. The extrudability and flowability of the PCL might be changed after dissolving in chloroform and mixing with GO powder. The interconnected pore structure, which facilitates the cell attachment and proliferation, of all the scaffolds, are clearly visible. Further, surface GO particles may facilitate the initial cell attachment.

3.3 *In vitro* cell culture

Figure 4 shows the live and dead cell assay images of scaffolds at days 3, 7, and 14. The cell attachment at day 3 on scaffolds are lower than day 7, and the significant difference was not observed within the groups. At day 14, whole scaffolds were covered with the cells, and few dead cells were also observed in all six groups. So, no toxicity was visible due to the GO and processing conditions. GO can be successfully incorporated into the PCL using this method without any cytotoxic effect. However, the cell viability and proliferation cannot be quantified using live/dead cell assay because of 3D nature and the interconnected pore structure of the scaffolds. Therefore, the WST-1 cell proliferation assay was used to overcome this problem.

Figure 5 shows the WST-1 cell proliferation assay results at days 3, 7, and 14. At day 3, no significant difference was observed between the groups for both 800 and 400 μm pore scaffolds. At day 3, 400 μm pore scaffolds showed high optical density value compare to 800 μm pore scaffolds, which represents the more cell attachment, but the differences were not statistically significant. Surprisingly, this behavior was not observable after day 3, as it shows similar values for both 800 μm and 400 μm pore scaffolds or the difference was not statistically significant ($p > 0.05$). The effect of pore size on cell proliferation was studied using DNA quantification assay, and the results are shown in the supplementary section. According to that results, porosity played a major role in initial cell attachment, but later the effect of porosity became insignificant. The incorporation of GO with PCL does not reduce the cell viability and cell proliferation as given in the results. According to Fig. 5, increasing the GO content increases cell proliferation as 0.5% GO scaffolds showed higher OD value compared to the 0.1% GO scaffolds. Mohammadi S et al. reported similar findings related to different GO concentration in PCL+GO fibrous scaffolds by using the methylthiazolyldiphenyl-tetra-sodium bromide (MTT) assay. Also, no significant increase in the cell viability in human osteoblastic sarcoma cell line was reported with the increasing GO content [30]. Further, Similar cell behavior was observed by the number of researchers using different cell types such as human bone marrow-derived mesenchymal stem cells [37,38], murine preosteoblasts [28], and rat bone marrow-derived mesenchymal stem cells [39].

The morphology of the attached cells is shown in the Fig.6. In general, the presence of GO did not influence the shape of the cells in comparison to PCL only scaffolds. At day 5, there were few attached cells on the scaffolds, and this further aligned with the previous L/D assay and WST-1 assay results. After day5, cells proliferated quickly and covered the scaffolds. At day 10, the usual elongated structure showed filopodia extensions, and cellular propagation fronts were observed in the cells. This observation suggests that the GO does not hamper the normal cell behavior and therefore the incorporation of GO into the scaffolds would not affect the physiological conditions of the microenvironment.

3.4 Cell Differentiation

The murine preosteoblasts can be induced to differentiate to osteoblasts in media supplemented with L-ascorbic acid (50 μg/ml), and β-glycerolphosphate (10 mM). After a predetermined period (at days 3, 7, and 14), of osteogenic induction, the extent of ALP

expression as assessed via ALP assay. The quantification of ALP activity within the cells attached to the scaffolds at days 3, 7, and 14 is shown in Fig. 7. The ALP activity of all the groups was increased with the time. In contrast to the 1 fold increase in day 7, 60 fold increase if ALP activity was observed compared to the day 3. At day 3, the ALP activity of GO contained scaffolds were lower than the PCL only scaffolds. However, at day 14, GO contained scaffolds showed high ALP activity with the increasing GO content. So, ALP levels of scaffolds at day 14 clearly proved the activation of osteogenesis in all samples. In particular, the ALP activity of 0.1% GO and 0.5% GO contained 800 μm pore scaffolds was significantly increased ($p<0.05$) as compared to the control PCL only scaffold. However, the increase of ALP activity in 400 μm pore scaffolds was not significant compared to the control PCL only scaffold. This result suggests that the GO increases the osteogenic differentiation of murine preosteoblasts.

The mineralization amount of the Ca and P was further studied using the EDX analysis. Since this method is a microscopic method and the values depend on the various factors such as surface area, the magnification, and the number of counts per scanning, all the factors were kept as constant or very close to each other. Three samples were scanned, and the average percentage values for the Ca and P were recorded from a total value of 100 including oxygen and calcium. Homogeneous Ca, and P deposition on the scaffolds were observed as shown in the Fig.8 which represents the elemental mapping of the selected scaffolds. According to the results shown in the Fig. 9, the Ca and P depositions were increased with the increasing GO content as similar to the ALP activity. Since ALP activity was reported on day 14, cell-attached scaffolds which stayed in osteogenic media at days 14 and 21 were studied. At day 21, Ca deposition was significantly increased in comparison to the day 14. This EDX quantification data has further supported the results which were taken from the ALP activity assay. It was also reported that the cell mineralization on the GO substrate began after 7 days which further aligned with our findings [40]. Enhanced osteogenic potential due to GO was previously reported in several literatures.

According to Song et al. [18], 0.3% (w/w) GO, and 0.5% (w/w) GO in PCL scaffolds enhanced the differentiation of mesenchymal stem cells into osteogenic cells. Wu D. et al. [29] also reported the enhanced bio-mineralization of the PCL scaffolds due to the GO addition.

On the other hand, PCL is also a good biocompatible and bioactive material which facilitates osteogenic differentiation as reported in the literature [41,42]. Because of this excellent behavior of the PCL, the significant statistical difference at $p < 0.05$ between groups cannot be observed. The finding of this project bolster the previous findings related to PCL and GO based scaffolds. Most importantly, this is the first study of incorporating GO into the PCL for 3D printing. Most of the previous studies focused on the development of GO incorporated PCL nanofibers by using the electrospinning method [18]. The GO content of this research work was determined according to the previously reported PCL+ GO nanofiber based studies. However, the authors suggest using a higher amount of GO in 3D printing to obtain a significant improvement in cell proliferation and differentiation.

Figure 10 shows the western blot analysis of the scaffolds. PCL + 0.1%GO group was omitted from this study according to the results of the previous experiments. The results show that both PCL only scaffolds and PCL + 0.5%GO scaffolds secrete osteogenesis related proteins namely; BMP-2, a growth factor which induces undifferentiated cells into bone tissues [43,44] and osteopontin, a non-collageneous glycoprotein in mineralized bone matrix [45]. The concentrations of BMP-2 and OPN increased with the time as shown in graphs A and B, but the no significant differences between the groups were observed. BMP-2 is regarded as having the most potential for bone regeneration, and it is already approved by the FDA (with BMP-7) for spinal fusion and non-union treatments [46]. Also, osteopontin plays an essential role in adhesion of bone cells to the mineralized matrix due to the availability of arginine-glycine-aspartate (RGD) motif [47]. As previously mentioned, PCL acts as an excellent osteoinductive substrate to the preosteoblasts with the 3D pore structure which also facilitates the secretion of osteogenic markers; BMP-2, and osteopontin; as shown in the experimental results. The effect of pore size on ECM formation and osteogenesis still not fully understood according to the results. At day 14, scaffolds with smaller pore size showed higher secretion of BMP2 and osteopontin, but the difference is not statistically significant at $p<0.05$ value.

We also concerned about the heating of GO incorporated PCL up to 100°C for printing, since it might effect to the biocompatibility of the GO due to the phase transformation. It was reported that the annealing of GO further improves the cell attachment, proliferation, and differentiation of human mesenchymal stem cells. During mild annealing of GO, there is a phase transformation toward distinct oxidized and graphitic domains. Also, the adsorption of ascorbic acid by annealed GO is higher than the adsorption of non-treated GO. Therefore, enhanced differentiation was observed in annealed GO [40]. Previous studies also have shown that the hydrogen bonding in the sp^3 carbon domain also could enhance the ascorbic acid adhesion performance of GO [35,37].

The available techniques to produce GO incorporated PCL scaffolds are limited. Electrospinning is the most widely used technique which can be found abundantly in literature as mentioned in the introduction section. However, the electrospinning method does not enable the precise control of internal scaffold architecture. On the other hand, 3D printing enables the better control of pore size, pore morphology, and porosity of the matrix [48,49] since interconnected pore structure is vital for cell nutrition, proliferation, and migration for the formation of new tissues and vascularization [50,51].

4. Conclusion

In this study, Go was successfully incorporated into the PCL using chloroform as a solvent and scaffolds were printed using the extrusion-based 3D printer. All types of scaffolds exhibited well-defined architecture and interconnected pore structure. The process conditions did not affect to the cytotoxicity of the scaffolds as murine preosteoblast attached and proliferated well on all three types of scaffolds. The addition of the GO enhanced the cellular response. The PCL+0.5% GO scaffold was the most favorable for cell proliferation and differentiation. Also, PCL was an ideal material for tissue engineering application as it enhanced the cell proliferation and differentiation, and GO further enhanced the cell

functions. We suggest that the 3D printed PCL/GO system has high potential as an artificial substitute for bone tissue engineering.

Supplementary Material

Refer to Web version on PubMed Central for supplementary material.

Acknowledgment

We would like to acknowledge National Institutes of Health (NIH) grant number R01DE023356 and the University of Toledo for financial support.

5. References

[1]. Woodfield TBF, Malda J, De Wijn J, Péters F, Riesle J, Van Blitterswijk CA, Design of porous scaffolds for cartilage tissue engineering using a three-dimensional fiber-deposition technique, Biomaterials. 25 (2004) 4149–4161. doi: 10.1016/j.biomaterials.2003.10.056. [PubMed: 15046905]

[2]. Hutmacher DW, Schantz T, Zein I, Ng KW, Teoh SH, Tan KC, Mechanical properties and cell cultural response of polycaprolactone scaffolds designed and fabricated via fused deposition modeling, J. Biomed. Mater. Res 55 (2001) 203–216. doi: 10.1002/1097-4636(200105)55:2<203::AID-JBM1007>3.0.CO;2-7. [PubMed: 11255172]

[3]. Park SA, Lee SH, Kim WD, Fabrication of porous polycaprolactone/hydroxyapatite (PCL/HA) blend scaffolds using a 3D plotting system for bone tissue engineering, Bioprocess Biosyst. Eng 34 (2011) 505–513. doi: 10.1007/s00449-010-0499-2. [PubMed: 21170553]

[4]. Trachtenberg JE, Placone JK, Smith BT, Piard CM, Santoro M, Scott DW, Fisher JP, Mikos AG, Extrusion-Based 3D Printing of Polypropylene fumarate) in a Full-Factorial Design, ACS Biomater. Sci. Eng 2 (2016) 1771–1780. doi:10.1021/acsbiomaterials.6b00026.

[5]. Tarafder S, Bose S, Polycaprolactone-coated 3D printed tricalcium phosphate scaffolds for bone tissue engineering: In vitro alendronate release behavior and local delivery effect on in vivo osteogenesis, ACS Appl. Mater. Interfaces 6 (2014) 9955–9965. doi:10.1021/am501048n. [PubMed: 24826838]

[6]. Li J, Chen M, Wei X, Hao Y, Wang J, Evaluation of 3D-printed polycaprolactone scaffolds coated with freeze-dried platelet-rich plasma for bone regeneration, Materials (Basel). 10 (2017). doi: 10.3390/mal0070831.

[7]. Hutmacher DW, Scaffold design and fabrication technologies for engineering tissues — state of the art and future perspectives, J. Biomater. Sci. Polym. Ed 12 (2001) 107–124. doi: 10.1163/156856201744489. [PubMed: 11334185]

[8]. Piard CM, Chen Y, Fisher JP, Cell-Laden 3D Printed Scaffolds for Bone Tissue Engineering, Clin. Rev. Bone Miner. Metab 13 (2015) 245–255. doi: 10.1007/s12018-015-9198-5.

[9]. Scaffaro R, Lopresti F, Botta L, Rigogliuso S, Ghersi G, Preparation of three-layered porous PLA/PEG scaffold: Relationship between morphology, mechanical behavior and cell permeability, J. Mech. Behav. Biomed. Mater 54 (2016) 8–20. doi:10.1016/j.jmbbm.2015.08.033. [PubMed: 26410761]

[10]. Shao W, He J, Sang F, Wang Q, Chen L, Cui S, Ding B, Enhanced bone formation in electrospun poly(l-lactic-co-glycolic acid)-tussah silk fibroin ultrafine nanofiber scaffolds incorporated with graphene oxide, Mater. Sci. Eng. C 62 (2016) 823–834. doi:10.1016/j.msec.2016.01.078.

[11]. Wendel B, Rietzel D, Kühnlein F, Feulner R, Hülder G, Schmachtenberg E, Additive processing of polymers, Macromol. Mater. Eng 293 (2008) 799–809. doi:10.1002/mame.200800121.

[12]. Dong L, Wang SJ, Zhao XR, Zhu YF, Yu JK, 3D-printed poly (ϵ-caprolactone) scaffold integrated with cell-laden chitosan hydrogels for bone tissue engineering, Sci. Rep 7 (2017) 4–12. doi: 10.1038/s41598-017-13838-7. [PubMed: 28127054]

[13]. Hoch E, Tovar GEM, Borchers K, Bioprinting of artificial blood vessels: Current approaches towards a demanding goal, Eur. J. Cardio-Thoracic Surg 46 (2014) 767–778. doi: 10.1093/ejcts/ezu242.

[14]. Li Z, Tan BH, Towards the development of polycaprolactone based amphiphilic block copolymers: Molecular design, self-assembly and biomedical applications, Mater. Sci. Eng. C 45 (2015) 620–634. doi:10.1016/j.msec.2014.06.003.

[15]. Wu D, Sun Y, Xu X, Cheng S, Zhang X, Zhuo R, Biodegradable and pH-Sensitive Hydrogels for Cell Encapsulation and Controlled Drug Release Biodegradable and pH-Sensitive Hydrogels for Cell, Society. 2 (2008) 1155–1162. doi: 10.1021/bm7010328.

[16]. Loh XJ, Yee BJH, Chia FS, Sustained delivery of paclitaxel using thermogelling poly(PEG/PPG/PCL urethane)s for enhanced toxicity against cancer cells, J. Biomed. Mater. Res. - Part A 100 A (2012) 2686–2694. doi: 10.1002/jbm.a.34198.

[17]. Rumiński S, Ostrowska B, Jaroszewicz J, Skirecki T, Włodarski K, Święszkowski W. Lewandowska-Szumieł M, Three-dimensional printed polycaprolactone-based scaffolds provide an advantageous environment for osteogenic differentiation of human adipose-derived stem cells, J. Tissue Eng. Regen. Med 12 (2018) e473–e485. doi: 10.1002/term.2310. [PubMed: 27599449]

[18]. Song J, Gao H, Zhu G, Cao X, Shi X, Wang Y, The preparation and characterization of polycaprolactone/graphene oxide biocomposite nanofiber scaffolds and their application for directing cell behaviors, Carbon N. Y 95 (2015) 1039–1050. doi: 10.1016/j.carbon.2015.09.011.

[19]. Chen H, Müller MB, Gilmore KJ, Wallace GG, Li D, Mechanically strong, electrically conductive, and biocompatible graphene paper, Adv. Mater 20 (2008) 3557–3561. doi: 10.1002/adma.200800757.

[20]. Rao CNR, Sood AK, Subrahmanyam KS, Govindaraj A, Graphene: The new two-dimensional nanomaterial, Angew. Chemie - Int. Ed 48 (2009) 7752–7777. doi: 10.1002/anie.200901678.

[21]. Fu C, Bai H, Zhu J, Niu Z, Wang Y, Li J, Yang X, Bai Y, Enhanced cell proliferation and osteogenic differentiation in electrospun PLGA/hydroxyapatite nanofibre scaffolds incorporated with graphene oxide, PLoS One. 12 (2017) e0188352. doi: 10.1371/joumal.pone.0188352. [PubMed: 29186202]

[22]. Rajesh R, Ravichandran YD, Development of new graphene oxide incorporated tricomponent scaffolds with polysaccharides and hydroxyapatite and study of their osteoconductivity on MG-63 cell line for bone tissue engineering, RSC Adv. 5 (2015) 41135–41143. doi: 10.1039/c5ra07015e.

[23]. Yıldırım S, Demirtaş TT. Dinçer CA, Yıldız N, Karakeçili A. Preparation of polycaprolactone/graphene oxide scaffolds: A green route combining supercritial CO2technology and porogen leaching, J. Supercrit. Fluids 133 (2018) 156–162. doi:10.1016/j.supflu.2017.10.009.

[24]. Shi X, Chang H, Chen S, Lai C, Khademhosseini A, Wu H, Regulating cellular behavior on few-layer reduced graphene oxide fdms with well-controlled reduction states, Adv. Funct. Mater 22 (2012) 751–759. doi: 10.1002/adfm.201102305.

[25]. Liu Z, Robinson JT, Sun X, Dai H, PEGylated Nano-Graphene Oxide for Delivery of Water Insoluble Cancer Drugs (b), J Am Chem Soc. 130 (2008) 10876–10877. doi: 10.1021/ja803688x. [PubMed: 18661992]

[26]. Li D, Kaner RB, Graphene-Based Materials Is Mars Geodynamically Dead ?, 320 (2008) 1170–1172.

[27]. La WG, Park S, Yoon HH, Jeong GJ, Lee TJ, Bhang SH, Han JY, Char K, Kim BS, Delivery of a therapeutic protein for bone regeneration from a substrate coated with graphene oxide, Small. 9 (2013) 4051–4060. doi:10.1002/smll.201300571. [PubMed: 23839958]

[28]. Hermenean A, Codreanu A, Herman H, Balta C, Rosu M, Mihali CV, Ivan A, Dinescu S, Ionita M, Costache M, Chitosan-Graphene Oxide 3D scaffolds as Promising Tools for Bone Regeneration in Critical-Size Mouse Calvarial Defects, Sci. Rep 7 (2017) 91–95. doi: 10.1038/s41598-017-16599-5. [PubMed: 28273893]

[29]. Wu D, Samanta A, Srivastava RK, Hakkarainen M, Nano-graphene oxide functionalized bioactive poly(lactic acid) and poly(ε-caprolactone) nanofibrous scaffolds, Materials (Basel). 11 (2018). doi: 10.3390/ma11040566.

[30]. Mohammadi S, Shafiei SS, Asadi-Eydivand M, Ardeshir M, Solati-Hashjin M, Graphene oxide-enriched poly(ϵ-caprolactone) electrospun nanocomposite scaffold for bone tissue engineering applications, J. Bioact. Compat. Polym 32 (2017) 325–342. doi: 10.1177/0883911516668666.

[31]. Sayyar S, Murray E, Thompson BC, Gambhir S, Officer DL, Wallace GG, Covalently linked biocompatible graphene/polycaprolactone composites for tissue engineering, Carbon N. Y 52 (2013) 296–304. doi:10.1016/j.carbon.2012.09.031.

[32]. Chaudhuri B, Bhadra D, Moroni L, Pramanik K, Myoblast differentiation of human mesenchymal stem cells on graphene oxide and electrospun graphene oxide-polymer composite fibrous meshes: Importance of graphene oxide conductivity and dielectric constant on their biocompatibility, Biofabrication. 7 (2015) 15009. doi: 10.1088/1758-5090/7/1/015009.

[33]. Chaudhuri B, Bhadra D, Mondal B, Pramanik K, Biocompatibility of electrospun graphene oxide-poly(ε-caprolactone) fibrous scaffolds with human cord blood mesenchymal stem cells derived skeletal myoblast, Mater. Lett 126 (2014) 109–112. doi:10.1016/j.matlet.2014.04.008.

[34]. Kang S, Park JB, Lee TJ, Ryu S, Bhang SH, La WG, Noh MK, Hong BH, Kim BS, Covalent conjugation of mechanically stiff graphene oxide flakes to three-dimensional collagen scaffolds for osteogenic differentiation of human mesenchymal stem cells, Carbon N. Y 83 (2015) 162–172. doi: 10.1016/j.carbon.2014.11.029.

[35]. Qi W, Yuan W, Yan J, Wang H, Growth and accelerated differentiation of mesenchymal stem cells on graphene oxide/poly-l-lysine composite films, J. Mater. Chem. B 2 (2014) 5461–5467. doi:10.1039/c4tb00856a.

[36]. Eshraghi S, Das S, Mechanical and microstructural properties of polycaprolactone scaffolds with one-dimensional, two-dimensional, and three-dimensional orthogonally oriented porous architectures produced by selective laser sintering, Acta Biomater. 6 (2010) 2467–2476. doi: 10.1016/j.actbio.2010.02.002. [PubMed: 20144914]

[37]. Lee WC, Lim CHYX, Shi H, Tang LAL, Wang Y, Lim CT, Loh KP, Origin of Enhanced Stem Cell Growth and Differentiation on Graphene and Graphene Oxide, ACS Nano. 5 (2011) 7334–7341. doi: 10.102l/nn202190c. [PubMed: 21793541]

[38]. Nayak TR, Andersen H, Makam VS, Khaw C, Bae S, Xu X, Ee PLR, Ahn JH, Hong BH, Pastorin G, Özyilmaz B, Graphene for controlled and accelerated osteogenic differentiation of human mesenchymal stem cells, ACS Nano. 5 (2011) 4670–4678. doi: 10.1021/nn200500h. [PubMed: 21528849]

[39]. Nie W, Peng C, Zhou X, Chen L, Wang W, Zhang Y, Ma PX, He C, Three-dimensional porous scaffold by self-assembly of reduced graphene oxide and nano-hydroxyapatite composites for bone tissue engineering, Carbon N. Y 116 (2017) 325–337. doi: 10.1016/j.carbon.2017.02.013.

[40]. Yang J-W, Hsieh KY, Kumar PV, Cheng S-J, Lin Y-R, Shen Y-C, Chen G-Y, Enhanced Osteogenic Differentiation of Stem Cells on Phase-Engineered Graphene Oxide, ACS Appl. Mater. Interfaces (2018) acsami.8b02225. doi:10.1021/acsami.8b02225.

[41]. Xue R, Qian Y, Li L, Yao G, Yang L, Sun Y, Polycaprolactone nanofiber scaffold enhances the osteogenic differentiation potency of various human tissue-derived mesenchymal stem cells, Stem Cell Res. Ther 8 (2017) 1–9. doi: 10.1186/s13287-017-0588-0. [PubMed: 28057078]

[42]. Ruckh TT, Kumar K, Kipper MJ, Popat KC, Osteogenic differentiation of bone marrow stromal cells on poly(ε-caprolactone) nanofiber scaffolds, Acta Biomater. 6 (2010) 2949–2959. doi: 10.1016/j.actbio.2010.02.006. [PubMed: 20144747]

[43]. Sun J, Li J, Li C, Yu Y, Role of bone morphogenetic protein-2 in osteogenic differentiation of mesenchymal stem cells, Mol. Med. Rep 12 (2015) 4230–4237. doi: 10.3892/mmr.2015.3954. [PubMed: 26096280]

[44]. Cao H, Liu X, Zhang X, Immunomodulatory Effects of Calcium and Strontium Co-Doped Titanium, Front. Immunol |. 8 (2017). doi: 10.3389/fimmu.2017.01196.

[45]. Hughes RC, Adhesive glycoproteins and receptors, Elsevier Masson SAS, 1997. doi:10.1016/S0167-7306(08)60627-4.

[46]. Davis HE, Case EM, Miller SL, Genetos DC, Leach JK, Engineering B, Davis UC, Osteogenic Response to BMP-2 of hMSCs Grown on Apatite-Coated Scaffolds, Biotechnol. Bioeng 108 (2011) 2727–2735. doi: 10.1002/bit.23227. [PubMed: 21656707]

[47]. Morinobu M, Ishijima M, Rittling SR, Tsuji K, Yamamoto H, Nifuji A, Denhardt DT, Noda M, Osteopontin Expression in Osteoblasts and Osteocytes During BoneFormation Under Mechanical Stress in the Calvarial Suture In Vivo, J. Bone Miner. Res 18 (2003) 1706–1715. [PubMed: 12968681]

[48]. Wu C, Luo Y, Cuniberti G, Xiao Y, Gelinsky M, Three-dimensional printing of hierarchical and tough mesoporous bioactive glass scaffolds with a controllable pore architecture, excellent mechanical strength and mineralization ability, Acta Biomater. 7 (2011) 2644–2650. doi:10.1016/j.actbio.2011.03.009. [PubMed: 21402182]

[49]. Loh QL, Choong C, Three-Dimensional Scaffolds for Tissue Engineering Applications: Role of Porosity and Pore Size, Tissue Eng. Part B Rev 19 (2013) 485–502. doi: 10.1089/ten.teb.2012.0437. [PubMed: 23672709]

[50]. Salerno A, Di Maio E, Iannace S, Netti PA, Tailoring the pore structure of PCL scaffolds for tissue engineering prepared via gas foaming of multi-phase blends, J. Porous Mater 19 (2012) 181–188. doi: 10.1007/s10934-011-9458-9.

[51]. Causa F, Netti PA, Ambrosio L, A multi-functional scaffold for tissue regeneration: The need to engineer a tissue analogue, Biomaterials. 28 (2007) 5093–5099. doi: 10.1016/j.biomaterials.2007.07.030. [PubMed: 17675151]

Highlights

- Graphene Oxide was successfully incorporated into Polycaprolactone using chloroform as a solvent
- Better interconnected and uniform porosity was obtained using the extrusion-based 3D printer.
- Scaffolds possessed good bioactivity, and graphene oxide increased the cell attachment and differentiation.
- Size of the pores does not influence the cell attachment significantly

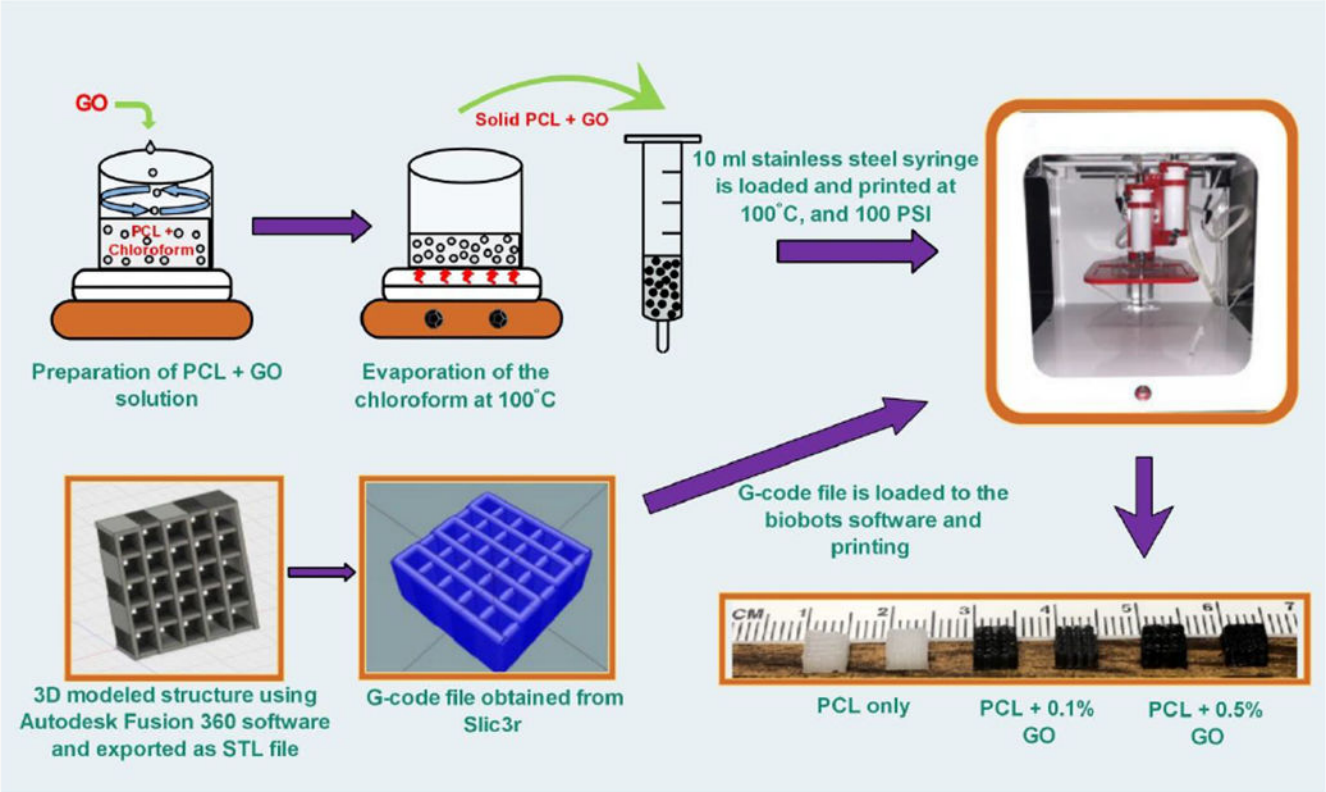

Figure 1:
Schematic representation of preparation of scaffolds using 3D printer

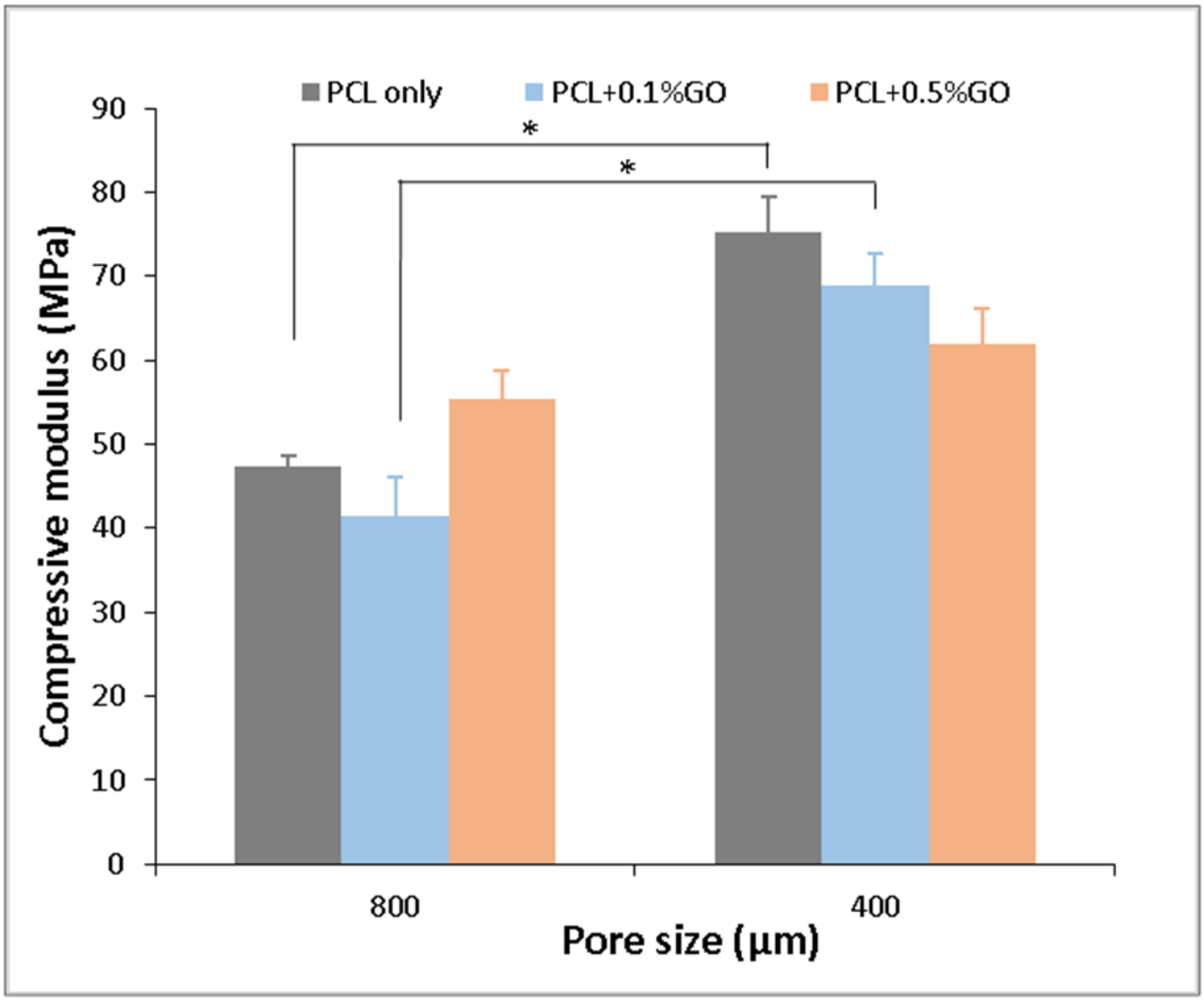

Figure 2:
Compressive modulus of scaffolds at two different pore sizes; * indicates $p<0.05$; n=7

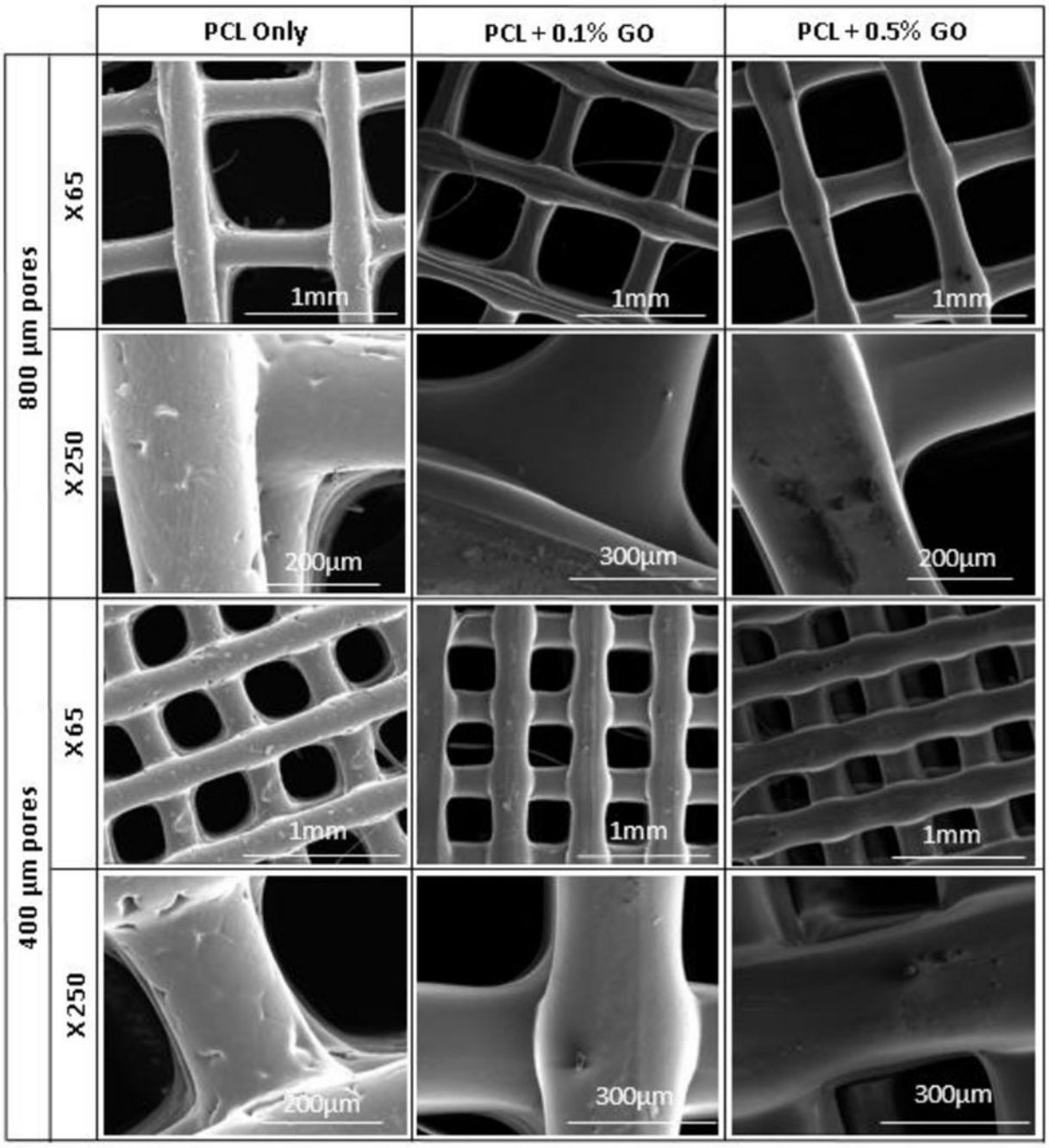

Figure 3:
SEM micrographs of scaffolds; X indicates the magnification

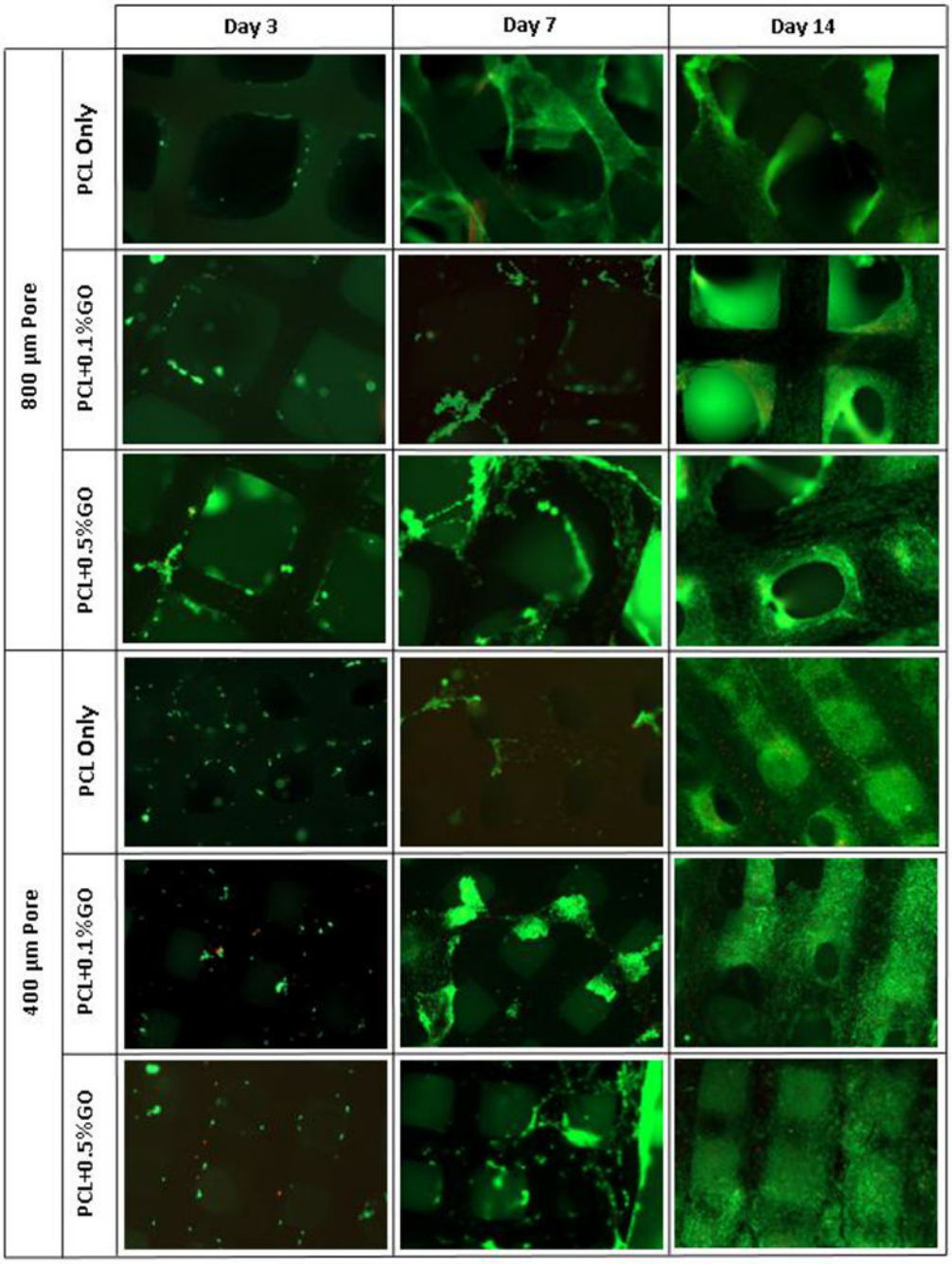

Figure 4:
Live and dead cell assay fluorescence images at days 3, 7, and 14; green- live cells, read-dead cells; scale 1 mm

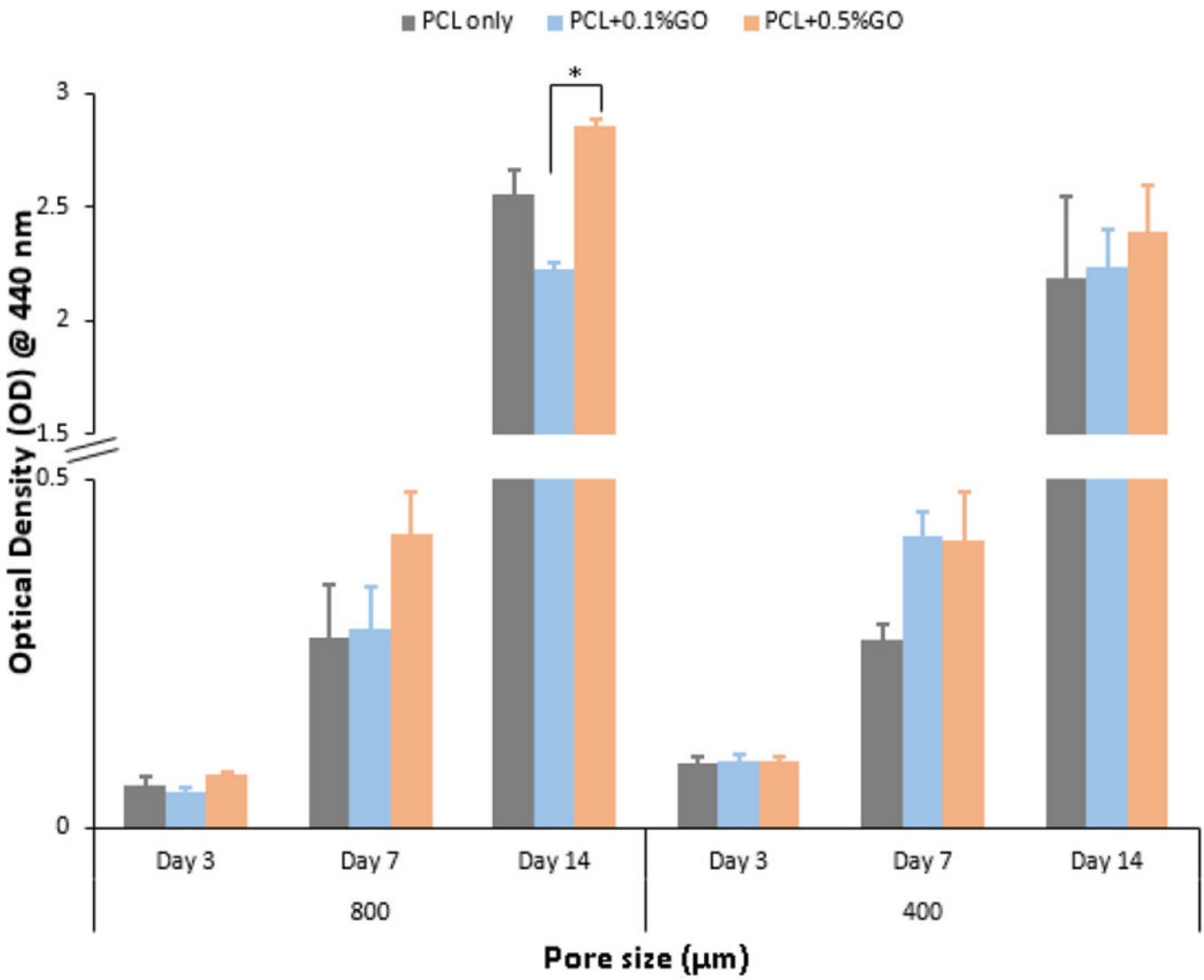

Figure 5:
WST-1 assay optical density values at 440 nm for three different time points; * indicates the $p<0.05$; n=3

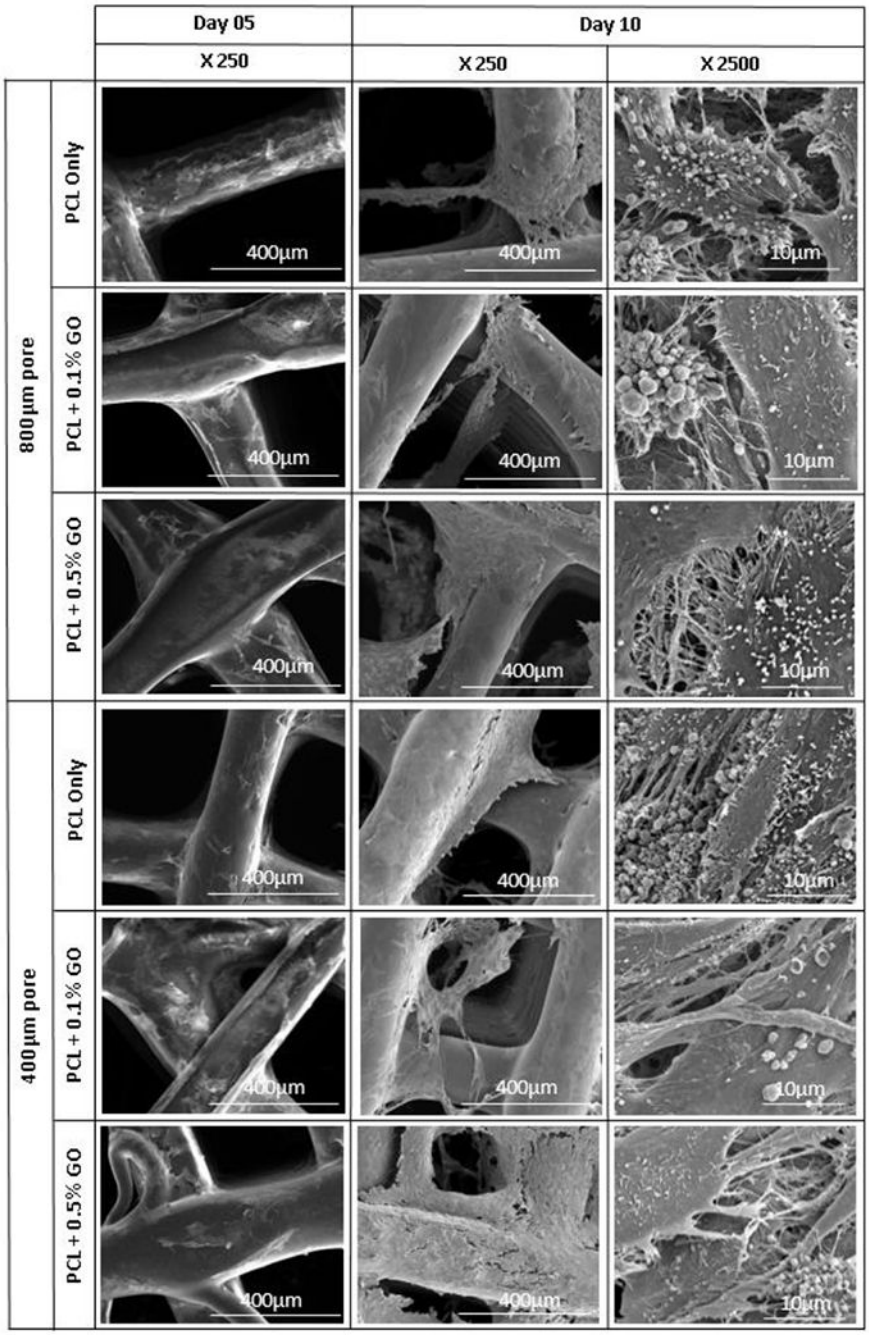

Figure 6:
SEM micrograph of osteoblast cell attachment at days 5 and 10; X indicates the magnification

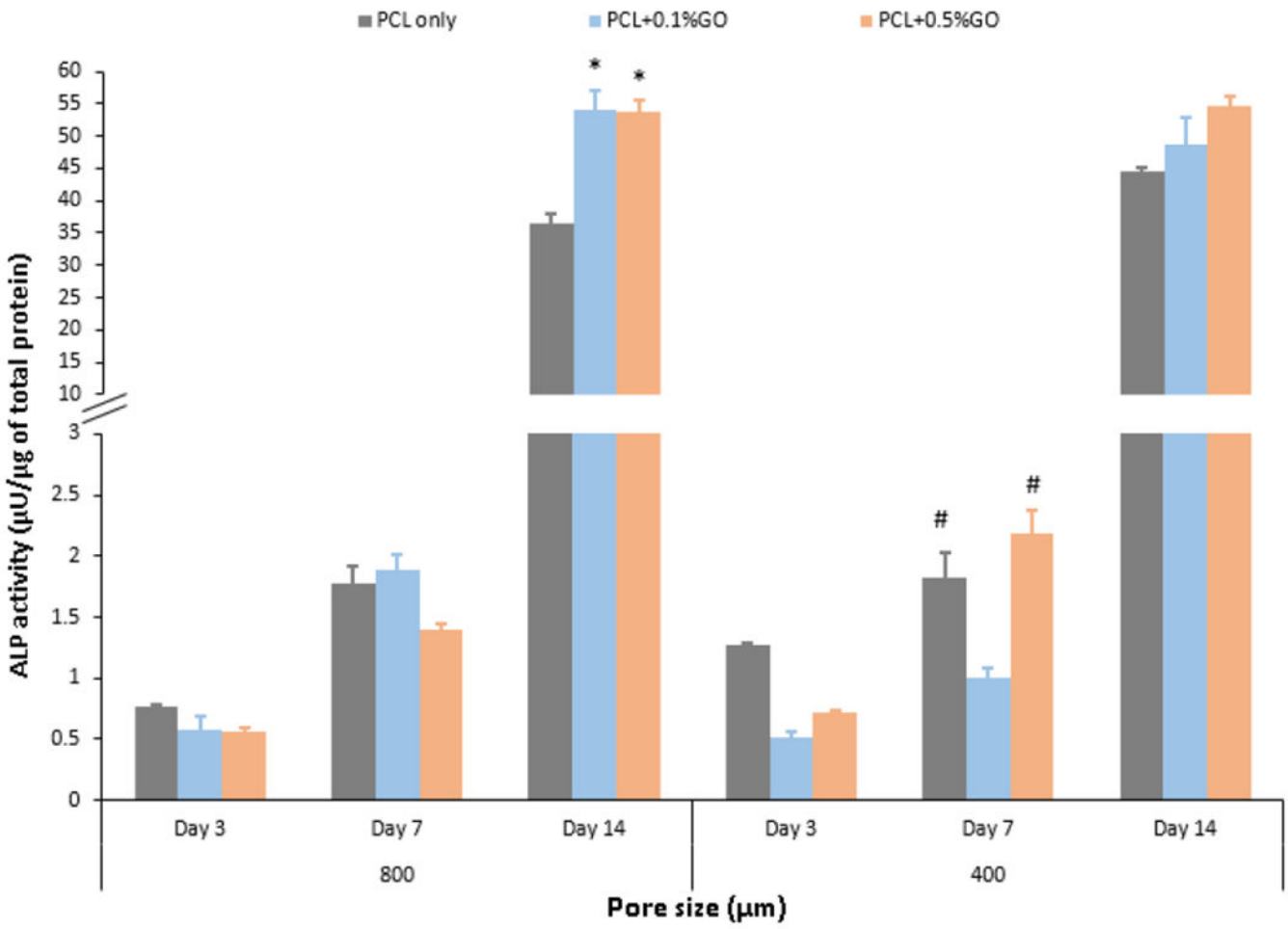

Figure 7:

ALP activity of the scaffolds at three different time points; * indicates the significance of $p<0.05$ with respect to (wrt) PCL only scaffold at day 14; # indicates the significance of $p<0.05$ wrt PCL +0.1% GO scaffold at day 7; n=3

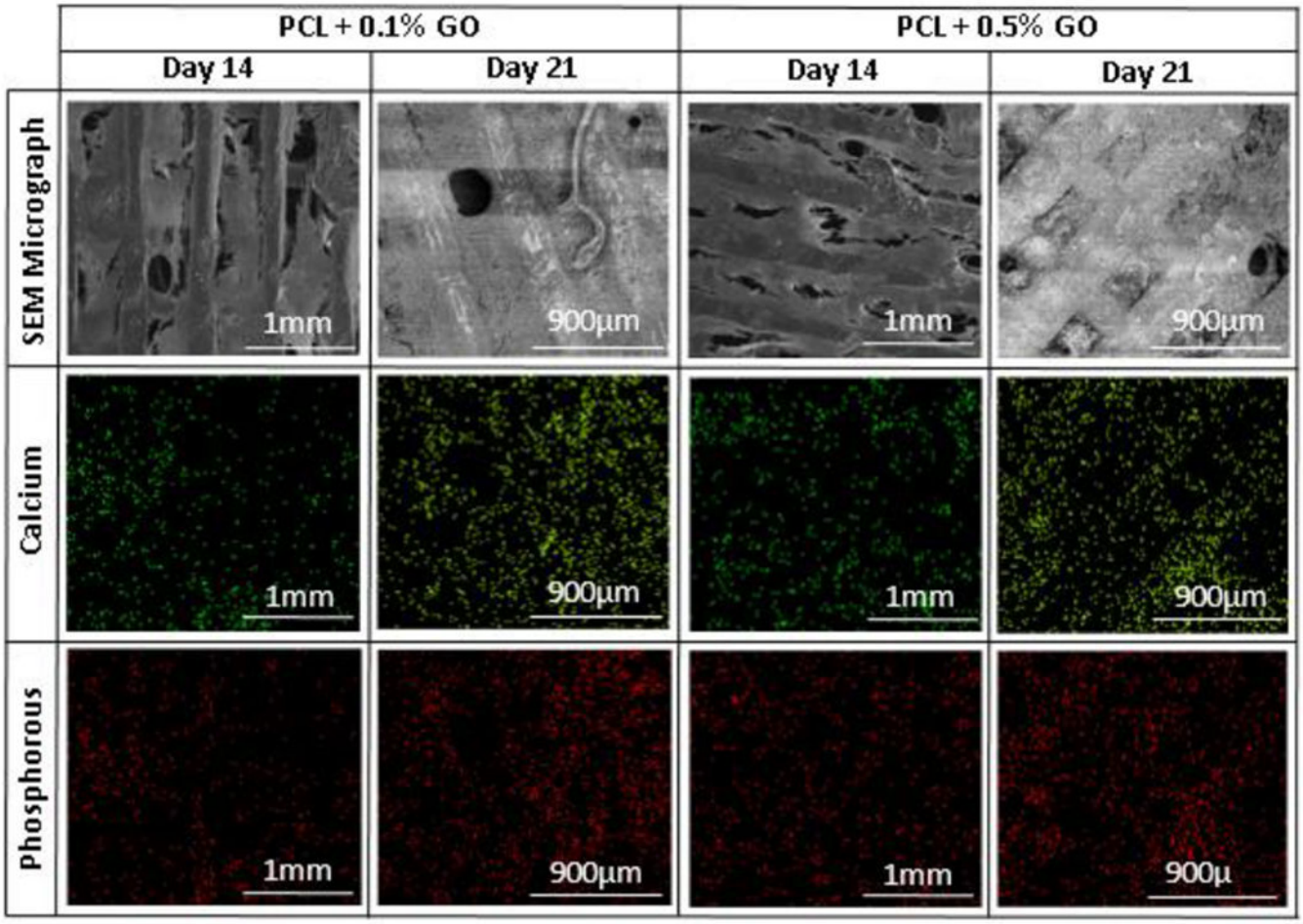

Figure 8:
Elemental mapping images and SEM micrographs of selected scaffolds after osteogenic differentiation at days 14 and 21

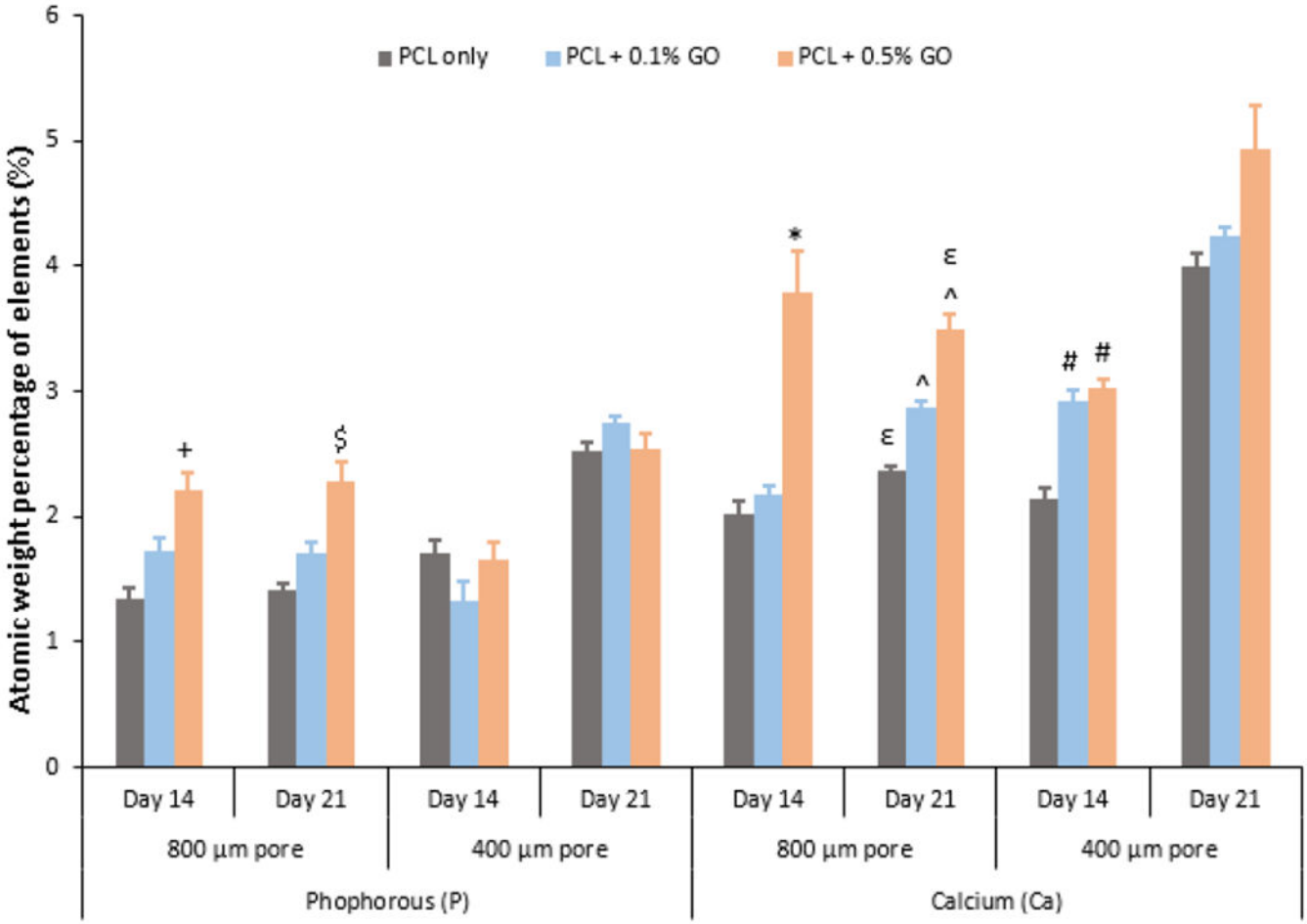

Figure 9:

Quantitative analysis of calcium and phosphorous elements using EDX method; + indicates the significance $p<0.05$ wrt PCL only; $ indicates the significance $p<0.05$ wrt PCL only; * indicates the significance $p<0.05$ wrt to both PCL only and PCL + 0.1% GO; ε indicates the significance $p<0.05$ wrt PCL + 0.1% GO; ^ indicates the significance $p<0.05$ wrt PCL only; # indicates the significance $p<0.05$ wrt PCL only

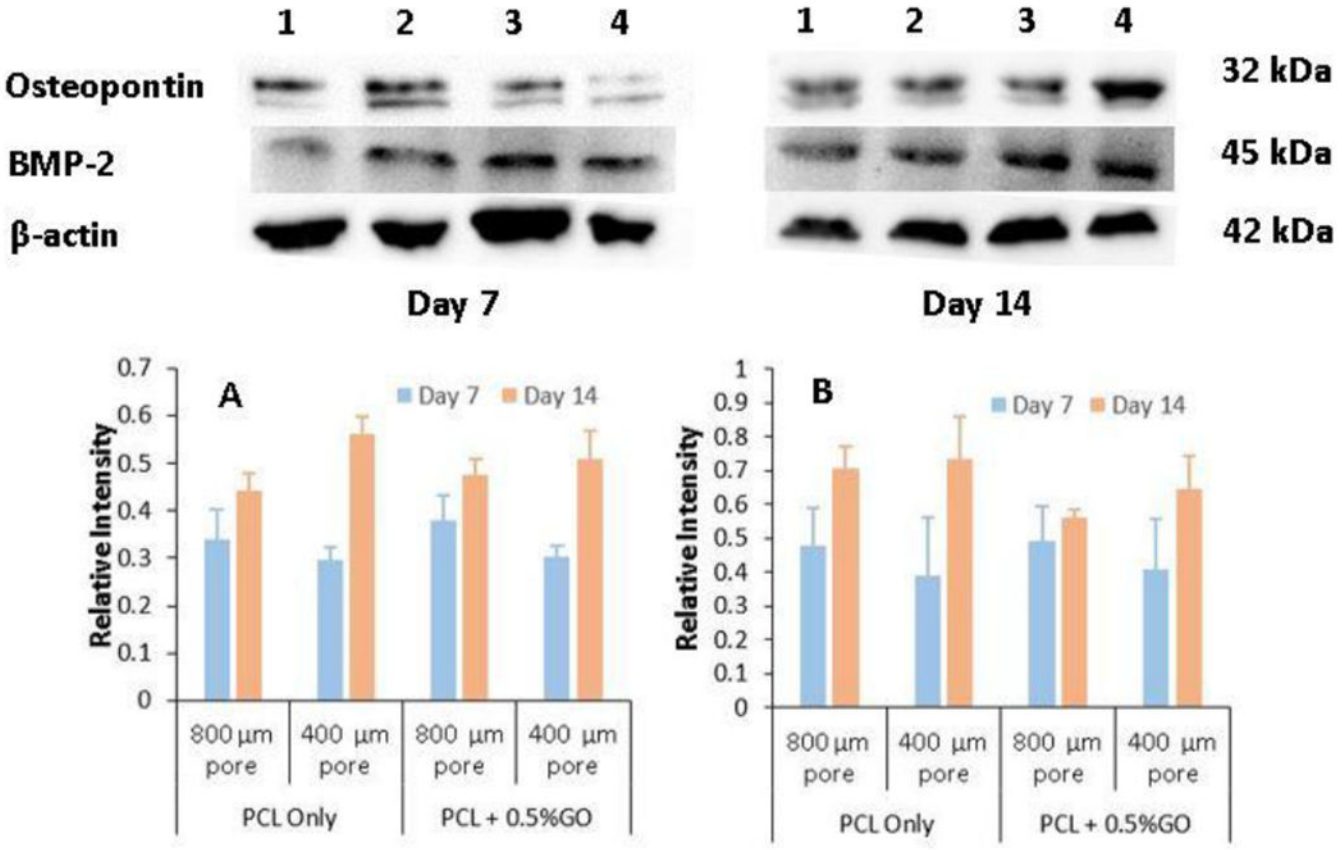

Figure 10:

Western blot analysis of preosteoblasts following the induction of osteogenic differentiation at day 7 and day 14 for different samples, 1- PCL only scaffolds with 800 µm pores, 2- PCL only scaffolds with 400 µm pores, 3- PCL + 0.5% GO scaffolds with 800 µm pores, and 4- PCL + 0.5% GO scaffolds with 400 µm pores; graph A: Bone Morphogenic Protein-2 (BMP-2), graph B: Osteopontin (OPN) (relative intensity wrt β-actin)